Journal of Power Sources 192 (2009) 693–697

Contents lists available at ScienceDirect

Journal of Power Sources

journal homepage: www.elsevier.com/locate/jpowsour

Short communication

Electrochemical performance of nanostructured spinel $LiMn_2O_4$ in different aqueous electrolytes

Lei Tian, Anbao Yuan*

Department of Chemistry, College of Sciences, Shanghai University, 99 Shangda Road, Shanghai 200444, PR China

ARTICLE INFO

Article history:
Received 9 January 2009
Received in revised form 26 February 2009
Accepted 2 March 2009
Available online 14 March 2009

Keywords:
Nanostructured spinel $LiMn_2O_4$
Room-temperature solid-state grinding reaction
Aqueous electrolyte
Li^+ insertion/abstraction
Electrochemical performance

ABSTRACT

A nanostructured spinel $LiMn_2O_4$ electrode material was prepared via a room-temperature solid-state grinding reaction route starting with hydrated lithium acetate ($LiAc{\cdot}2H_2O$), manganese acetate ($MnAc_2{\cdot}4H_2O$) and citric acid ($C_6H_8O_7{\cdot}H_2O$) raw materials, followed by calcination of the precursor at 500 °C. The material was characterized by X-ray diffraction (XRD) and transmission electron microscope techniques. The electrochemical performance of the $LiMn_2O_4$ electrodes in 2 M Li_2SO_4, 1 M $LiNO_3$, 5 M $LiNO_3$ and 9 M $LiNO_3$ aqueous electrolytes was studied using cyclic voltammetry, ac impedance and galvanostatic charge/discharge methods. The $LiMn_2O_4$ electrode in 5 M $LiNO_3$ electrolyte exhibited good electrochemical performance in terms of specific capacity, rate dischargeability and charge/discharge cyclability, as evidenced by the charge/discharge results.

© 2009 Elsevier B.V. All rights reserved.

1. Introduction

Compared with layered $LiCoO_2$ and $LiNiO_2$ intercalation compounds, spinel $LiMn_2O_4$ has the advantages of naturally abundant, low cost, less toxic and facile preparation, and has attracted great attentions as an alternative positive electrode material for nonaqueous electrolyte lithium ion batteries [1–3]. However, its cycle stability is poor (especially at higher temperatures) due to Jahn–Teller distortion and manganese dissolution into electrolyte during cycling. For this reason, researchers attempt to improve its cycle stability using various approaches, such as surface coating [4,5], chemical doping [6,7], etc. Although nonaqueous organic electrolyte has the feature of wide electrochemical window, it has also the drawbacks of flammability, low conductivity and high cost. Whereas, aqueous electrolyte has the advantages of high conductivity and low cost. In 1994, Li and Dahn first reported a lithium ion battery with $LiMn_2O_4$ positive electrode, VO_2 negative electrode and 5 M $LiNO_3$ aqueous electrolyte [8]. Thereafter, studies on Li^+ ion batteries with aqueous electrolytes received interests gradually [9–26]. Some are concerned with the preparation and electrochemical properties of $LiMn_2O_4$ in Li^+ ions that contained aqueous electrolytes [11,13–18,21,22,26], and the others are concerned with aqueous Li^+ ion batteries [9,12,20,23–25] or supercapacitor [19] in the presence of $LiMn_2O_4$ as the positive electrodes. In these studies, various aqueous electrolytes were used, such as 3–9 M $LiNO_3$ [8,9,11–14,16,18,21–26], 1 M LiCl [15], 1 M or 2 M Li_2SO_4 [19,20] and $LiCF_3SO_3$ [21]. However, no comparative study of electrochemical performance of $LiMn_2O_4$ electrode in different aqueous electrolytes and no long-term cycling (full cycling) of $LiMn_2O_4$ electrode were reported. Besides, few studies about electrochemical properties of nanostructured $LiMn_2O_4$ in aqueous electrolyte was reported up to now. In 2000, Li et al. [13] studied the rate capability of $LiMn_2O_4$ nanotube (with different sizes of 150, 230 and 400 nm) electrodes in saturated aqueous $LiNO_3$ (~9 M) solution. This study demonstrated that the rate capability improved with decreasing wall thickness of the tubules which formed the electrode.

In the present work, a nanostructured spinel $LiMn_2O_4$ material was prepared via a room-temperature solid-state grinding reaction route starting with lithium acetate ($LiAc{\cdot}2H_2O$), manganese acetate ($MnAc_2{\cdot}4H_2O$) and citric acid ($C_6H_8O_7{\cdot}H_2O$), followed by calcination of the precursor at 500 °C. This is a facile preparation method which is distinguished from the commonly used high-temperature solid-state reaction or sol–gel technique reported in most literatures. The electrochemical performance of the $LiMn_2O_4$ electrode in different aqueous electrolytes was investigated with an emphasis on full charge/discharge cycling.

2. Experimental

2.1. Preparation and characterization of nanostructured $LiMn_2O_4$ material

$LiAc{\cdot}2H_2O$, $Mn(Ac)_2{\cdot}4H_2O$ and $C_6H_8O_7{\cdot}H_2O$ with molar ratio of 1:2:3 were ground in a mortar for about 1 h at ambient

* Corresponding author. Tel.: +86 21 66134851; fax: +86 21 66132797.
E-mail address: abyuan@shu.edu.cn (A. Yuan).

0378-7753/$ – see front matter © 2009 Elsevier B.V. All rights reserved.
doi:10.1016/j.jpowsour.2009.03.002

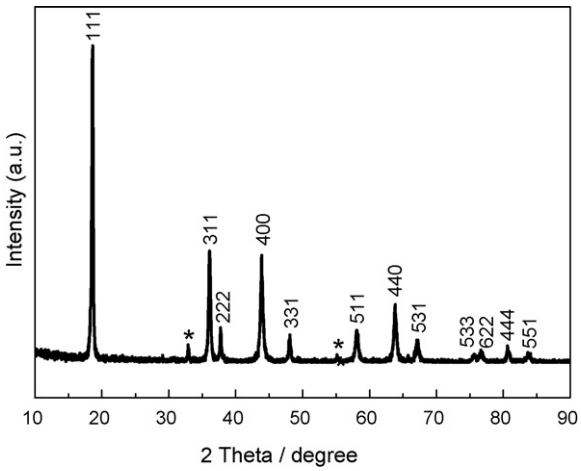

Fig. 1. XRD pattern of $LiMn_2O_4$ material.

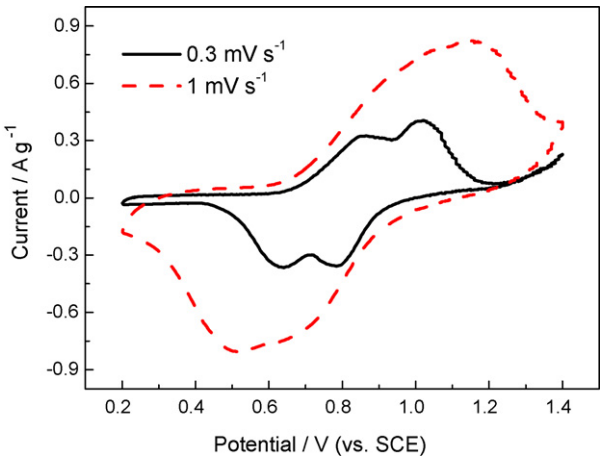

Fig. 3. CVs of $LiMn_2O_4$ electrodes in 2 M Li_2SO_4 solution at different scan rates.

temperature. In the grinding process, a solid-state reaction took place, accompanying with crystalline water releasing gradually, causing the reaction system wet and pasty. The pasty substance was treated in a water bath of 80 °C for 4 h, and then a precursor was obtained. The precursor was calcined at 500 °C for 12 h, and then the $LiMn_2O_4$ product was obtained.

X-ray diffraction (XRD) analysis of the $LiMn_2O_4$ material was conducted on a Rigaku D/max–2000 X-ray powder diffractometer with a Cu Kα radiation (40 kV, 250 mA) over the 2θ range of 10–90° at a scan rate of 0.02° s^{-1}. Morphological observation of the material was carried out using a JEOL JEM–200CX transmission electron microscope.

2.2. Fabrication and electrochemical testing of $LiMn_2O_4$ electrodes

$LiMn_2O_4$ electrodes were fabricated as follows: $LiMn_2O_4$ active material, acetylene black conductor and polytetrafluoroethylene binder with weight ratio of 75:20:5 were mixed thoroughly to form slurry. The slurry was coated onto a titanium mesh current collector with an apparent area of 1 cm × 1 cm, dried at 80 °C for 12 h, and then roll-pressed to ca. 0.7 mm thick.

Electrochemical measurements of the $LiMn_2O_4$ electrodes were performed in a three-electrode configuration glass cell, with $LiMn_2O_4$ and activated carbon as working and counter electrodes, respectively, and saturated calomel electrode (SCE) as reference electrode. 2 M Li_2SO_4, 1 M $LiNO_3$, 5 M $LiNO_3$ and 9 M $LiNO_3$ aqueous solutions with pH values of 5.81, 5.71, 5.56, and 5.34, respectively, were used as electrolytes. Cyclic voltammetry and ac impedance measurements were carried out using a Solartron instrument Model 1287 coupled with a 1255B FRA. The impedance spectra were measured at discharged state with open circuit potentials of 0.6052, 0.6672, 0.6097 and 0.3049 V (SCE) for the electrodes in 2 M Li_2SO_4, 1 M $LiNO_3$, 5 M $LiNO_3$ and 9 M $LiNO_3$ solutions, respectively. Charge/discharge tests were conducted using a LAND auto-cycler (China). All the tests were conducted at 30 °C.

3. Results and discussion

3.1. XRD analysis and TEM observation of $LiMn_2O_4$ material

Fig. 1 shows the XRD pattern of the $LiMn_2O_4$ material. The diffractions occurred at 2θ = 18.62°, 36.08°, 37.72°, 43.88°, 48.12°, 58.30°, 63.86°, 67.10°, 75.64°, 76.80°, 80.62° and 83.72° should be indexed to the characteristic diffractions of spinel $LiMn_2O_4$ (PDF 35–0782). In addition, two faint diffraction peaks at 32.86° and 55.14° corresponding to the strongest diffractions of Mn_2O_3 (PDF 78–0390, 73–1826, 71–0636, 71–0635) can be observed. XRD result demonstrates that the obtained material belongs to face-centered cubic spinel $LiMn_2O_4$ (space group: $Fd3m$, cell parameters: a = 8.247 Å) with trace amounts of Mn_2O_3 phase.

Fig. 2(a) and (b) shows the TEM images of the $LiMn_2O_4$ material with different magnifications. It can be seen from Fig. 2(a) that the material is composed of particles with a wide size distribution, about 20 nm to 1 μm. As can be seen in Fig. 2(b), the larger submicronic particles are aggregates of nanoscale crystallites less than

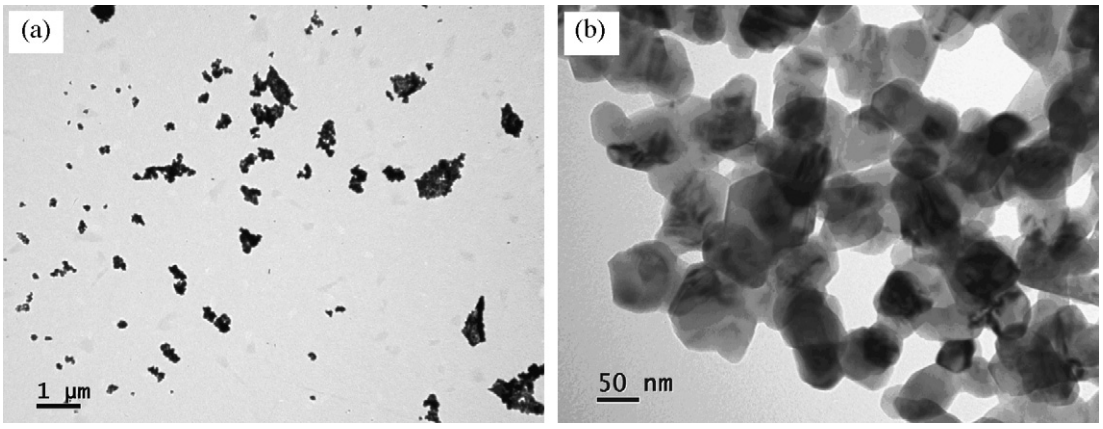

Fig. 2. TEM images of $LiMn_2O_4$ material with different magnifications.

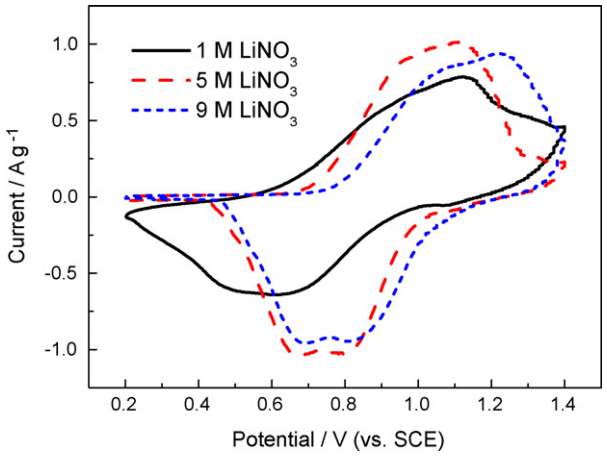

Fig. 4. CVs of $LiMn_2O_4$ electrodes in different $LiNO_3$ solutions at 1 mV s^{-1}.

100 nm. Based on the data of full width at half maximum (FWHM) of the characteristic diffractions in XRD and Scherrer's formula $D = 0.89\lambda/B\cos\theta$, the average size of the crystallites is estimated to be about 50 nm. This further indicates that the larger particles shown in TEM photographs are aggregates of nanoscale crystallites.

3.2. Electrochemical studies of $LiMn_2O_4$ electrodes in different aqueous electrolytes

Fig. 3 shows the cyclic voltammographs (CVs) of the $LiMn_2O_4$ electrodes in 2 M Li_2SO_4 solution at different scan rates. The current responses are obtained based on the mass of the $LiMn_2O_4$ active material. As can be seen, at the low scan rate of 0.3 mV s^{-1}, two couples of reversible redox peaks can be observed, which is consistent with the reports in literatures [13,15,18,21,22]. The anodic and cathodic peaks of the lower potential couple occur at 0.85 and 0.63 V (SCE), respectively, and those of the higher potential couple occur at 1.02 and 0.78 V, respectively. The Li^+ ions abstraction/insertion reaction of the $LiMn_2O_4$ electrode can be expressed as:

$$LiMn_2O_4 \rightleftharpoons Li_{1-x}Mn_2O_4 + xLi^+ + xe^- \quad (0 \le x \le 1)$$

the two couples of redox peaks should be attributed to Li^+ ions abstraction from/insertion into two different lattice sites in $LiMn_2O_4$ [26], which are similar to the behaviors of $LiMn_2O_4$ electrodes in nonaqueous electrolytes in the corresponding potential range [2,3]. The lower potential redox peaks correspond to Li^+ abstraction and insertion over the x value range of $0 \le x \le 0.5$ in $Li_xMn_2O_4$, and the higher potential redox peaks correspond to Li^+ abstraction and insertion over the x value range of $0.5 \le x \le 1$ [13].

However, when the scan rate is increased to 1 mV s^{-1}, the two couples of redox peaks are overlapped, and hence only one couple of wide redox peaks can be observed. Besides, the anodic and cathodic peak potentials shift toward positive and negative directions, respectively, and the peak currents are obviously increased. Judging from the shape of the CVs obtained either at 0.3 or at 1 mV s^{-1}, a good symmetry is exhibited for the oxidation and reduction processes. In addition, the onset potential of oxygen evolution shifts from ca. 1.2 to 1.4 V when the scan rate is increased from 0.3 to 1 mV s^{-1}. This can be explained as follows: when the electrode is charged to higher potentials, the Li^+ deintercalation will compete with the oxygen evolution. When the scan rate is increased from 0.3 to 1 mV s^{-1}, the increment of overpotential of oxygen evolution is larger than that of Li^+ deintercalation owing to the different kinetics of the two reactions. Hence, it follows that the oxygen evolution could be delayed at higher scan rates.

Fig. 4 shows the CVs of the $LiMn_2O_4$ electrodes in 1 M, 5 M and 9 M $LiNO_3$ solutions, respectively at 1 mV s^{-1}. As can be seen, the $LiMn_2O_4$ electrodes in different concentrations of $LiNO_3$ solutions exhibit obvious redox current peaks, but show different characteristics. In 1 M $LiNO_3$ solution, only one couple of redox peaks can be observed. This couple of wide redox peaks should be ascribed to overlap of two couples of redox peaks as similar to the case in 2 M Li_2SO_4 solution (see Fig. 3). However, in 5 M and 9 M $LiNO_3$ solutions, two distinguishable adjacent reduction peaks can be observed, while the corresponding two oxidation peaks are difficult to be distinguished. Compared with the CVs in 1 M $LiNO_3$ or in 2 M Li_2SO_4 solutions, the reduction peak potentials are obviously moved forward, and the redox currents are increased markedly. In 9 M $LiNO_3$ solution, the oxidation peak potential is also moved forward. Compared with Fig. 3, the peak current response of the electrode in 5 M or 9 M $LiNO_3$ solution is larger than that in 2 M Li_2SO_4 solution at the identical scan rate of 1 mV s^{-1}, and the peak current response in 1 M $LiNO_3$ solution is lower than that in 2 M Li_2SO_4 solution. The above results suggest that the reversibility of the electrode reaction in 5 M or 9 M $LiNO_3$ solution is much superior to that in 1 M $LiNO_3$ or 2 M Li_2SO_4 solution. As seen by the difference between the peak potentials of oxidation and reduction, the reaction reversibility of the electrode in 5 M $LiNO_3$ solution is the best.

Fig. 5 displays the Nyquist plots of the $LiMn_2O_4$ electrodes in different electrolytes. The impedance values (in Ω g) are based on the mass of $LiMn_2O_4$, and the inset is the close up view of the ac impedance in high-frequency region. As can be seen, the ac impedance spectra obtained in different electrolytes consist of a high-frequency arc and a low-frequency line. This observation is similar to the ac impedance spectra of $LiMn_2O_4$ thin film electrodes in $LiNO_3$ solutions [18,21]. The high-frequency arc should be attributed to charge transfer process whose size reflects the charge transfer resistance, and the low-frequency line corresponds to diffusion process of Li^+ ions in $LiMn_2O_4$ solid [18,21]. With decreasing frequency, the slope angle of the line is increased from the initial value of ca. 45° to an almost vertical line, exhibiting a diffusion characteristic of a porous electrode other than an ideal Warburg semi-infinite diffusion. This suggests that the Li^+ ion diffusion in bulk $LiMn_2O_4$ proceeds quickly [21], which is likely related to the nanostructure of the $LiMn_2O_4$ material. The ohmic resistance in 5 M or in 9 M $LiNO_3$ solution is less than that in 1 M $LiNO_3$ or in 2 M Li_2SO_4 solution, due to the higher conductivity of 5 M or 9 M $LiNO_3$ solution. The charge transfer resistance in 5 M or in 9 M $LiNO_3$ solution is small, which is increased a little in 2 M Li_2SO_4 solution, and

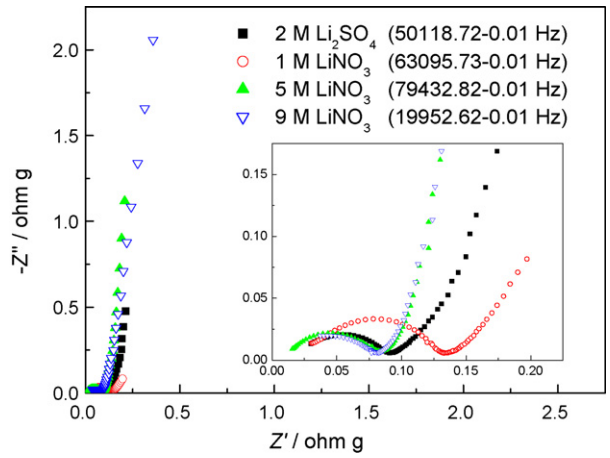

Fig. 5. Nyquist plots of $LiMn_2O_4$ electrodes measured at discharged state with open circuit potentials of 0.6052, 0.6672, 0.6097 and 0.3049 V (SCE) in 2 M Li_2SO_4, 1 M $LiNO_3$, 5 M $LiNO_3$ and 9 M $LiNO_3$ solutions, respectively.

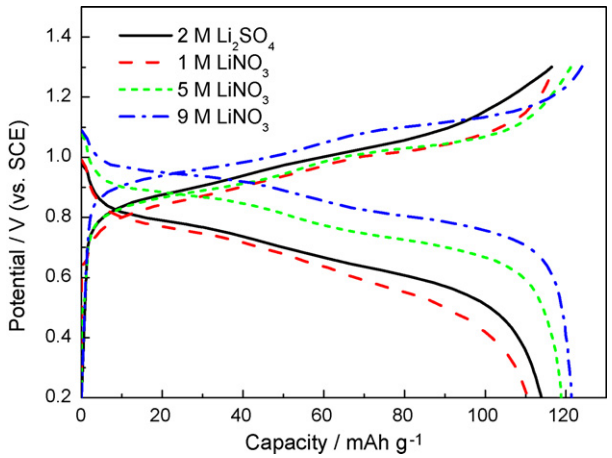

Fig. 6. Charge and discharge profiles of $LiMn_2O_4$ electrodes in different electrolytes at a current rate of 500 mA g^{-1}.

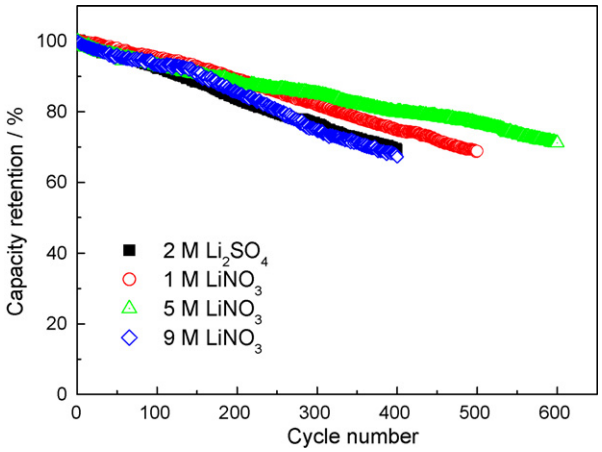

Fig. 8. Charge/discharge cycle-life profiles of $LiMn_2O_4$ electrode in different electrolytes at a current rate of 500 mA g^{-1}.

while, the charge transfer resistance is increased remarkably in 1 M $LiNO_3$ solution. These results suggest that the electrolyte can not only influence the ohmic resistance but also influence the charge transfer resistance of the electrode.

Fig. 6 shows the charge and discharge profiles of the $LiMn_2O_4$ electrodes in different electrolytes at the current rate of 500 mA g^{-1} (based on the mass of $LiMn_2O_4$) over the operating potential range of 0.2–1.3 V (SCE). In 5 M or in 9 M $LiNO_3$ solutions, two distinguishable potential plateaus for charging or discharging can be observed, corresponding to the two couples of redox peaks observed in the CVs (see Fig. 4). While, in 1 M $LiNO_3$ or in 2 M Li_2SO_4 solution, no distinguishable plateau could be observed. This is because that the high-rate reversibility of the electrode in 5 M or in 9 M $LiNO_3$ solution is superior to that in 1 M $LiNO_3$ or in 2 M Li_2SO_4 solution, as revealed by the CV results. Higher charge/discharge current rates correspond to higher scan rates in CV. At higher current rates, the reaction reversibility of the electrode in 1 M $LiNO_3$ or in 2 M Li_2SO_4 solution becomes poor. In addition, the charge and discharge potentials in 9 M $LiNO_3$ solution are higher than those in 5 M $LiNO_3$ solution, which is consistent with the observed peak potentials in CVs (see Fig. 4). The charge/discharge specific capacities and the discharge potentials of the electrode in different electrolytes follow the order: 9 M $LiNO_3$ > 5 M $LiNO_3$ > 2 M Li_2SO_4 > 1 M $LiNO_3$.

Fig. 7 shows the discharge specific capacities of the $LiMn_2O_4$ electrode in different electrolytes at different charge/discharge current rates over the operating potential range of 0.2–1.3 V (SCE). As

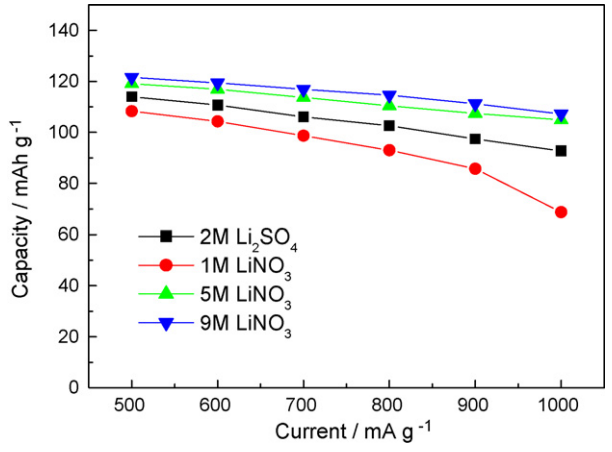

Fig. 7. Discharge specific capacities of $LiMn_2O_4$ electrodes in different electrolytes at different current rates.

can be seen, in the current range of 500–1000 mA g^{-1}, the specific capacities of the electrodes in different solutions decrease with current rate increasing, but show different fading magnitudes. For example, when the current rate is increased from 500 to 1000 mA g^{-1}, the specific capacities of the electrodes in 2 M Li_2SO_4, 1 M $LiNO_3$, 5 M $LiNO_3$ and 9 M $LiNO_3$ solutions are decreased from 114.0, 108.3, 119.1 and 121.6 mAh g^{-1} to 92.7, 68.7, 104.9 and 107.2 mAh g^{-1}, i.e., decreased by 18.6%, 36.6%, 11.9% and 11.8%, respectively. The rate capabilities follow the order: 9 M $LiNO_3$ > 5 M $LiNO_3$ > 2 M Li_2SO_4 > 1 M $LiNO_3$, which is in agreement with the ac impedance results in Fig. 5. That is to say, the rate dischargeability decreases with the electrode impedance increasing. As can be seen, at any a current rate, the specific capacities follow the order: 9 M $LiNO_3$ > 5 M $LiNO_3$ > 2 M Li_2SO_4 > 1 M $LiNO_3$. The above results indicate that the $LiMn_2O_4$ electrode in 5 M or in 9 M $LiNO_3$ solution has higher specific capacity and discharge potential as well as better rate dischargeability, which is likely related to the Li^+ ions activities and conductivities of the different electrolytes. In Ref. [26], the discharge specific capacities of the $LiMn_2O_4$ electrode in 5 M $LiNO_3$ electrolyte at $C/1.5$, $2C$, $3C$, $4C$ and $7C$ rates were reported to be ca. 73, 69, 67, 61 and 52 mAh g^{-1}, respectively. The theoretical capacity of $LiMn_2O_4$ electrode is ca. 148 mAh g^{-1} (x = 0–1 in $Li_{1-x}Mn_2O_4$). In the present work, the specific capacities of the $LiMn_2O_4$ electrode in 5 M $LiNO_3$ electrolyte at 500, 600, 700, 800, 900 and 1000 mA g^{-1} rates (corresponding to about $3.4C$, $4.1C$, $4.7C$, $5.4C$, $6.1C$ and $6.8C$, respectively, based on the theoretical capacity) are 119.1, 116.9, 113.7, 110.4, 107.4 and 104.9 mAh g^{-1}, respectively. The specific capacity and rate capability of the $LiMn_2O_4$ electrode in this work are higher than those reported [26].

Fig. 8 shows the charge/discharge cycle-life profiles of the $LiMn_2O_4$ electrodes in different electrolytes at the current rate of 500 mA g^{-1} over the operating potential range of 0.2–1.3 V (SCE). In the initial 150 cycles, no significant difference in cycling stability between the different electrolytes could be observed. However, after 150 cycles the difference appeared gradually. The electrode in 5 M $LiNO_3$ solution presents the best cycling stability with capacity retention of 71.2% after 600 cycles. The cycling stability in 1 M $LiNO_3$ solution takes the second place, with capacity retention of 68.8% after 500 cycles. In 2 M Li_2SO_4 and in 9 M $LiNO_3$ solutions, the capacity retentions are 69.3% and 67.2%, respectively, after 400 cycles, presenting the poor cycling stabilities. In general, the electrode in 5 M $LiNO_3$ solution presents the best electrochemical performance, with not only higher initial specific capacity and good rate dischargeability, but also better cycling stability.

Owing to the superior electrochemical performance of the $LiMn_2O_4$ electrode in 5 M $LiNO_3$ solution, it can be used as posi-

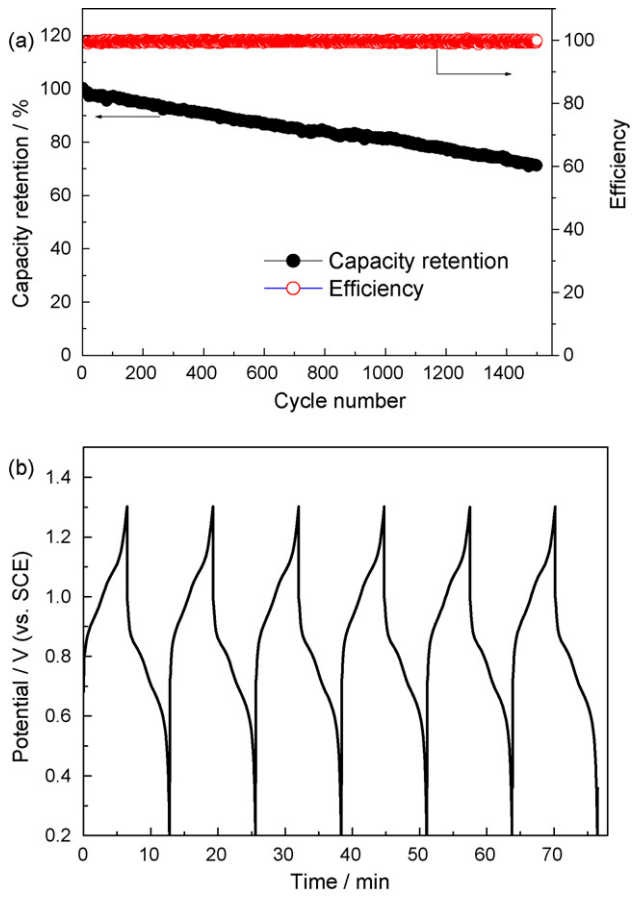

Fig. 9. Cycle life (a) and charge/discharge profile (b) of $LiMn_2O_4$ electrode in 5 M $LiNO_3$ electrolyte at a high current rate of 1000 mA g^{-1}.

tive electrodes for aqueous lithium ion batteries or supercapacitors, for example, $LiMn_2O_4$/activated carbon capacitors. Fig. 9(a) shows the cycle life and current efficiency of the $LiMn_2O_4$ electrode in 5 M $LiNO_3$ electrolyte at the high current rate of 1000 mA g^{-1}, and Fig. 9(b) shows the charge/discharge profile of initial several cycles. At this high current rate, the initial specific capacity is ca. 105 mAh g^{-1}, corresponding to an average specific capacitance of 344 F g^{-1} over the potential range of 0.2–1.3 V (SCE). As can be seen in Fig. 9(b), the electrode potential drops fast after discharged to 0.5 V, that is to say, in the potential range of 0.5–0.2 V, the dischargeable capacity is low. If we calculate based on the actual discharge capacity over the discharge potential range of 1.3–0.5 V, the average specific capacitance over the potential range of 1.3–0.5 V can reach a high value of 473 F g^{-1}. As can be seen in Fig. 9(a), after 1500 cycles, the capacity retention can maintain at 71.3%, exhibiting a superior cycling stability than cycled at 500 mA g^{-1}. Besides, a high charge/discharge current efficiency of ca. 100% can be achieved.

4. Conclusions

The $LiMn_2O_4$ electrode material was prepared using a room-temperature solid-state reaction route starting with $LiAc{\cdot}2H_2O$, $MnAc_2{\cdot}4H_2O$ and $C_6H_8O_7{\cdot}H_2O$ followed by calcination. XRD revealed that the material is spinel $LiMn_2O_4$ with trace amounts of Mn_2O_3 phase. The material is composed of particles ranged from ca. 20 nm to 1 μm, and the submicronic particles are aggregates of nanoscale crystallites, as demonstrated by TEM observation. Electrochemical results indicated that the $LiMn_2O_4$ electrodes in different electrolytes can show different specific capacities, rate dischargeabilities and charge/discharge cyclabilities. The electrode in 5 M $LiNO_3$ solution exhibited the best electrochemical performance, with high specific capacity, good rate dischargeability and good cyclability, which would be used as a promising positive electrode for aqueous lithium ion batteries or supercapacitors.

Acknowledgement

This work was supported by Leading Academic Discipline Project of Shanghai Municipal Education Commission (Project Number: J50102).

References

[1] V.G. Kumar, J.S. Gnanaraj, S. Ben-David, D.M. Pickup, E.R.H. van-Eck, A. Gedanken, D. Aurbach, Chem. Mater. 15 (2003) 4211.
[2] C.H. Jiang, S.X. Dou, H.K. Liu, M. Ichihara, H.S. Zhou, J. Power Sources 172 (2007) 410.
[3] T. Doi, T. Yahiro, S. Okada, J. Yamaki, Electrochim. Acta 53 (2008) 8064.
[4] H.W. Ha, N.J. Yun, K. Kim, Electrochim. Acta 52 (2007) 3236.
[5] H. Şahan, H. Göktepe, S. Patat, A. Ülgen, Solid State Ionics 178 (2008) 1837.
[6] J.M. Amarilla, R.M. Rojas, F. Pico, L. Pascual, K. Petrov, D. Kovacheva, M.G. Lazarraga, I. Lejona, J.M. Rojo, J. Power Sources 174 (2007) 1212.
[7] L.F. Xiao, Y.Q. Zhao, Y.Y. Yang, Y.L. Cao, X.P. Ai, H.X. Yang, Electrochim. Acta 54 (2008) 545.
[8] W. Li, J.R. Dahn, D.S. Wainwright, Science 264 (1994) 1115.
[9] W. Li, J.R. Dahn, J. Electrochem. Soc. 142 (1995) 1742.
[10] M.J. Zhang, J.R. Dahn, J. Electrochem. Soc. 143 (1996) 2730.
[11] P. Wang, H. Yang, H.Q. Yang, J. Power Sources 63 (1996) 275.
[12] G.X. Wang, S. Zhong, D.H. Bradhurst, S.X. Dou, H.K. Liu, J. Power Sources 74 (1998) 198.
[13] N.C. Li, C.J. Patrissi, G.L. Che, C.R. Martin, J. Electrochem. Soc. 147 (2000) 2044.
[14] A. Eftekhari, Electrochim. Acta 47 (2001) 495.
[15] T. Grygar, P. Bezdička, P. Piszora, J. Solid State Electrochem. 5 (2001) 487.
[16] K.S. Abou-El-Sherbini, M.H. Askar, J. Solid State Electrochem. 7 (2003) 435.
[17] M. Jayalakshmi, M.M. Rao, F. Scholz, Langmuir 19 (2003) 8403.
[18] J.W. Lee, S.-I. Pyun, Electrochim. Acta 49 (2004) 753.
[19] Y.G. Wang, Y.Y. Xia, Electrochem. Commun. 7 (2005) 1138.
[20] G.J. Wang, H.P. Zhang, L.J. Fu, B. Wang, Y.P. Wu, Electrochem. Commun. 9 (2007) 1873.
[21] N. Nakayama, T. Nozawa, Y. Iriyama, T. Abe, Z. Ogumi, K. Kikuchi, J. Power Sources 174 (2007) 695.
[22] N. Cvjeticanin, I. Stojkovic, M. Mitric, S. Mentus, J. Power Sources 174 (2007) 1117.
[23] J.Y. Luo, Y.Y. Xia, Adv. Funct. Mater. 17 (2007) 3877.
[24] H.B. Wang, K.L. Huang, Y.Q. Zeng, S. Yang, L.Q. Chen, Electrochim. Acta 52 (2007) 3280.
[25] H.B. Wang, Y.Q. Zeng, K.L. Huang, S.Q. Liu, L.Q. Chen, Electrochim. Acta 52 (2007) 5102.
[26] N.N. Sinha, P. Ragupathy, H.N. Vasan, N. Munichandraiah, Int. J. Electrochem. Sci. 3 (2008) 691.